

**Deep follow-up of GW151226: ordinary binary or low-mass-ratio system?**AVI VAJPEYI,<sup>1,2</sup> RORY SMITH,<sup>1,2</sup> AND ERIC THRANE<sup>1,2</sup><sup>1</sup>*School of Physics and Astronomy, Monash University, VIC 3800, Australia*<sup>2</sup>*OzGrav: The ARC Centre of Excellence for Gravitational Wave Discovery, Monash University, VIC 3800, Australia***ABSTRACT**

Recent work by Chia *et al.* [arxiv/2105.06486] raises questions about the nature of the binary black hole event GW151226. While LIGO–Virgo initially determined this event to be an “ordinary” merger with a modest mass ratio  $q \equiv m_2/m_1 = 7.5M_\odot/14M_\odot$  and modest effective inspiral spin  $\chi_{\text{eff}} \approx 0.15$ , Chia *et al.* find support for a far more interesting system: with a significant mass asymmetry  $q \approx 4.3M_\odot/29M_\odot$ , substantial spin  $\chi_{\text{eff}} \approx 0.5$ , and signs of Lense–Thirring precession. Chia *et al.* find that the “low- $q$ ” likelihood peak is preferred over the high- $q$  peak with a posterior odds of  $\mathcal{O} \approx 96$  while LIGO–Virgo find the low- $q$  peak is *disfavored* with an odds of  $\mathcal{O} \approx 8$  (meaning the two studies differ by a ratio of  $\approx 770$ ). This discrepancy has been challenging to resolve since Chia *et al.* argue that the low- $q$  peak is present only when the data are analyzed with substantial computing resources. In this *Letter* we introduce a “deep follow-up” framework to efficiently compute the posterior odds between two different points in parameter space: in this case, one corresponding to the “high- $q$ ” LIGO–Virgo peak and one corresponding to the “low- $q$ ” peak identified by Chia *et al.* We find the high- $q$  interpretation is barely preferred with a posterior odds of  $\sim 1.2$ , suggesting that GW151226 may well be an unusual (low- $q$ ) event, though, it is equally well explained as an ordinary merger. If it is a low- $q$  merger, it is a remarkable event with a large primary black hole spin  $\chi_1 \sim 0.88^{+0.11}_{-0.14}$ , at least partly tilted into the orbital plane. However, the data are not informative enough to distinguish between this interpretation or a more vanilla black hole binary. This result implies that the LIGO–Virgo analysis did not adequately sample parameter space. At the same time, we find less evidence for a low- $q$  peak than reported by Chia *et al.* We discuss strategies to produce more reliable parameter estimation studies in gravitational-wave astronomy.

**1. INTRODUCTION**

The binary black hole merger GW151226 was the second gravitational-wave event detected (Abbott *et al.* 2016). The LIGO–Virgo–Kagra (LVK) collaboration (LIGO Scientific Collaboration *et al.* 2015; Acernese *et al.* 2015) measured the event with a signal to noise ratio  $\text{SNR} \sim 13$ , source-frame masses of  $(m_1, m_2) = (14.2^{+8.3}_{-3.7}M_\odot, 7.5^{+2.3}_{-2.3}M_\odot, 90\% \text{ credibility})$  and with the mass ratio  $q \equiv m_2/m_1$  consistent with unity (Abbott *et al.* 2016).<sup>1</sup> The event was noteworthy at the time of detection because—unlike GW150914, the first gravitational-wave detection—GW151226 showed signs

of black hole spin. The effective inspiral parameter,

$$\chi_{\text{eff}} \equiv \frac{\chi_1 \cos \theta_1 + q \chi_2 \cos \theta_2}{1 + q} \quad (1)$$

is a measure of the black hole spin projected onto the orbital angular momentum axis.<sup>2</sup> This parameter was found to be inconsistent with zero at high credibility  $\chi_{\text{eff}} = 0.18^{+0.25}_{-0.08}$ , suggesting that at least one of the black holes in GW151226 was measurably spinning (Abbott *et al.* 2016). A subsequent analysis by Mateu-Lucena *et al.* (2021) draws a similar conclusion using a more sophisticated gravitational waveform than what was available for the initial analysis (Pratten *et al.* 2021). These results suggest GW151226 is a fairly typical merger; most events in the LIGO–Virgo gravitational-wave transient catalog (Abbott *et al.* 2021) are consistent with

avi.vajpeyi@monash.edu

<sup>1</sup> Here, the subscript 1 refers to the primary, more massive black hole while the 2 refers to the less massive secondary.<sup>2</sup> Here,  $\chi_{1,2}$  are the dimensionless black-hole spins and  $\theta_{1,2}$  are the tilt angles between the spin vectors and the orbital angular momentum vector.

$q = 1$  and approximately 20% exhibit signs of measurable spin (Roulet et al. 2021; Galadage et al. 2021).

However, Chia et al. (2021) suggest this interpretation of GW151226 is incomplete. They reanalyzed GW151226 and found a low- $q$  likelihood peak with  $(m_1, m_2) = (29.3_{-11.0}^{+11.4} M_\odot, 4.3_{-0.8}^{+1.7} M_\odot)$  with a ln-likelihood six points higher than the high- $q$  peak identified by the LVK. Due to the degeneracy between  $q$  and  $\chi_{\text{eff}}$ , the low- $q$  peak is associated with a larger effective inspiral spin  $\chi_{\text{eff}} = 0.50_{-0.25}^{+0.14}$ . The Chia *et al.* interpretation makes GW151226 a more interesting event. With a highly asymmetric mass ratio  $q = 0.15_{-0.06}^{+0.18}$ , GW151226 is less like typical events in GWTC-3 (Abbott et al. 2021) and more like the mysterious GW190814 (Abbott et al. 2020a)—an event which is difficult to explain in the context of standard binary evolution. In order to simultaneously achieve such a large value of  $\chi_{\text{eff}}$  and a small value of  $q$ , the primary black hole must have non-zero spin (Qin et al. 2022). However, this is somewhat challenging to explain in the usual framework of tidal interactions, which serve to spin up only the second-born (typically less massive) black hole (Mandel & Fragos 2020).<sup>3</sup> Finally, Chia *et al.* suggest that GW151226 exhibits clear signs of Lense-Thirring precession, which would make this the first system to exhibit clearly this affect (Green et al. 2021; Abbott et al. 2021).

Given the exciting implications of the Chia *et al.* results, it is important to understand why this result differs from the original LVK result (Abbott et al. 2016) and the more recent analysis by Mateu-Lucena et al. (2021). (A third analysis by Nitz et al. (2021) failed to break the stalemate—obtaining results broadly consistent with Mateu-Lucena et al. (2021) while simultaneously finding some support for a low- $q$  peak.) Since both Chia *et al.* and Mateu-Lucena et al. (2021) use the same gravitational waveform in their analyses, Chia *et al.* speculate that the difference is due to the fact that they employ a large number of nested-sampling live points are needed to accurately explore the parameter space, which increases the computational cost of the analysis.<sup>4</sup> They suggest 15,000 (roughly an order of magnitude greater than typically used in LVK analyses) are required to obtain a well-converged result. This

creates a predicament: the community has two conflicting results, and computationally expensive analyses are required in order to reproduce one of the analyses.

In this Letter we demonstrate a method to resolve the tension between two different sets of parameter estimation results. We apply this technique to GW151226 in order to settle the debate on the relative importance of the low- $q$  and high- $q$  likelihood peaks. We compute the marginal likelihood of two points in the  $q - \chi_{\text{eff}}$  distribution, one from the low- $q$  likelihood peak and another from the high- $q$  peak. By restricting the analysis to the two-dimensional  $q - \chi_{\text{eff}}$  space, we reduce the dimensionality of the problem, permitting a “deep follow-up” investigation on the  $q - \chi_{\text{eff}}$  modes of GW151226 without the need for large computational resources. While we demonstrate this method on GW151226, the same principles can be applied to resolve other discrepancies in the gravitational-wave astronomy literature. The remainder of this letter is organized as follows. In Section 2, we describe the “deep follow-up” formalism used to compute our posterior odds. Then, in Section 3, we show results obtained from a deep follow-up of GW151226. We provide closing comments in Section 4.

## 2. METHODOLOGY

Different analyses may find different peaks in the marginal likelihood distribution. In this section we provide a mathematical method to determine which peak is more probable than another. We label the two disparate likelihood peaks  $A$  and  $B$  and ask the question: what are the posterior odds of hypothesis  $A$  over hypothesis  $B$ ? If this odds, denoted  $\mathcal{O}_B^A$ , is much larger (or much smaller) than unity ( $\ln \mathcal{O} \gg 8$  or  $\ln \mathcal{O} \ll -8$ ), then one hypothesis can be said to be strongly preferred over the other. When this happens, we may conclude that one hypothesis provides a better description of the posterior distribution.<sup>5</sup> On the other hand if  $\mathcal{O} \approx 1$ , this implies that both hypotheses are approximately equally consistent with the data. When this happens, we may conclude that one or more analysis is incomplete insofar as it did not produce both a posterior consistent with both  $A$  and  $B$ .

In the case of GW151226, we choose  $A$  and  $B$  from peaks in the  $(q, \chi_{\text{eff}})$  plane, because different peaks in this plane can lead to unique physical interpretations of the event. As we are only interested in this plane, the marginal likelihood distribution  $\mathcal{Z}(d|q, \chi_{\text{eff}})$  allows us to focus on just the 2 parameters at a time; the other

<sup>3</sup> In some events, large primary spin can arise due to the phenomenon of “mass ratio reversal” (Olejak & Belczynski 2021), though, this seems unlikely to have occurred in a system with such a small mass ratio.

<sup>4</sup> There are other subtle differences, which we explore in greater detail below. These include: different initial prior distributions (which can affect sampler efficacy), different stochastic samplers, different noise estimation techniques, different sampling frequencies, and different methods for likelihood estimation.

<sup>5</sup> More precisely, one hypothesis is preferred over the other given whatever assumptions we have made constructing our likelihood function.

parameters (e.g., total mass, the effective precession parameter, etc.) are integrated out. By fixing the parameter values associated with points  $A$  and  $B$  we reduce the dimensionality of our inference calculation, which improves convergence; for our GW151226 analysis, the dimensionality of the marginalized likelihood is reduced by two. Moreover, we do not have to worry about our stochastic sampler failing to find peaks  $A$  and  $B$ —we force the sampler to study just these two points in parameter space. By setting up the problem this way, we give up trying to map the full  $(q, \chi_{\text{eff}})$  subspace, focusing our computational power so that we obtain reliable estimates of the marginal likelihood at just the two points  $A$  and  $B$ . If the original inference calculations by Abbott et al. (2016) and Chia et al. (2021) are analogous to all-sky searches, this analysis is analogous to a deep follow-up study.

The posterior odds are

$$\mathcal{O}_B^A = \frac{Z(d|A)}{Z(d|B)} \frac{\pi(A)}{\pi(B)}, \quad (2)$$

where  $Z(d|...)$  refers to the marginal likelihood for hypothesis  $A$  or  $B$  and  $\pi(...)$  refers to the prior odds for hypothesis  $A$  or  $B$ . The marginal likelihood for point  $A$  or  $B$  is given by

$$Z(d|A, B) = \int \mathcal{L}(d|\theta) \pi(\theta|A, B), \quad (3)$$

where  $\mathcal{L}(d|\theta)$  is the usual Whittle likelihood used in gravitational-wave astronomy (see, e.g., Thrane & Talbot (2019)) and  $\pi(\theta|A, B)$  is the prior on  $\theta$  conditioned upon hypothesis  $A, B$ . We first discuss how to calculate the marginal likelihood and then describe how to calculate the prior odds.

*The marginal likelihood.* Our first step is to define the priors conditioned on hypotheses  $A, B$ . In this study,  $\pi(\theta|A, B)$  is the fiducial LIGO–Virgo prior from Abbott et al. (2016), conditioned on  $(q, \chi_{\text{eff}})_{A, B}$ , the location of either the high- $q$  peak associated with the original LVK study Abbott et al. (2016) or the low- $q$  peak identified by Chia et al. (2021). The fiducial LIGO–Virgo prior is uniform in: the dimensionless spin parameters  $\chi_1, \chi_2$ , the azimuthal angle of the spin vectors  $\phi_1, \phi_2$ , and the cosine of the spin-vector zenith angle  $z_1, z_2$ . Following Mateu-Lucena et al. (2021), the prior distribution of black hole masses is uniform in  $(m_1, m_2)$  over the interval  $(3M_\odot, 54M_\odot)$  subject to the constraint that  $m_2 < m_1$ . We employ a uniform-in-comoving volume prior for luminosity distance and assume standard priors for the other extrinsic parameters.

The next step is to condition the original prior on  $(q, \chi_{\text{eff}})_{A, B}$ . Using Eq. 1, we can express our prior on

$\chi_{\text{eff}}$  as delta function:

$$\pi(\chi_{\text{eff}}|\chi_1, z_1, z_2, \chi_2, q_{A, B}) = \delta\left(\chi_{\text{eff}} - \frac{\chi_1 z_1 + q_{A, B} \chi_2 z_2}{1 + q_{A, B}}\right). \quad (4)$$

Here,  $q_{A, B}$  refer to the mass ratio associated with either hypothesis  $A$  or hypothesis  $B$ . By changing variables, we obtain a conditional prior on  $\chi_2$  for hypotheses  $A$  and  $B$ :

$$\pi(\chi_2|\chi_1, z_1, z_2)_{A, B} = \delta\left(\chi_2 - \frac{\chi_{\text{eff}}^{A, B}(1 + q_{A, B}) - \chi_1 z_1}{q_{A, B} z_2}\right). \quad (5)$$

Combining our fiducial prior with Eq. 5, we obtain the marginal prior distribution for  $\chi_1$  conditioned on  $A, B$ <sup>6</sup>

$$\begin{aligned} \pi(\chi_1)_{A, B} &= \int dz_1 dz_2 d\chi_2 \pi(\chi_1, z_1, z_2, \chi_2)_{A, B} \\ &= \int dz_1 dz_2 d\chi_2 \pi(\chi_1, z_1, z_2) \pi(\chi_2|\chi_1, z_1, z_2)_{A, B} \\ &\propto \frac{1}{n} \sum_k^n \mathcal{I}\left(0 < \frac{\chi_{\text{eff}}^{A, B}(1 + q_{A, B}) - \chi_1 z_1^k}{q_{A, B} z_2^k} < 1\right) \end{aligned} \quad (6)$$

In order to obtain the final expression, we wrote the integrals over  $z_1, z_2$  as a sum over prior samples drawn from the  $\pi(z_1)$  and  $\pi(z_2)$  distributions. The symbol  $\mathcal{I}$  denotes an indicator function, which returns zero when its argument is false and one when it's argument is true. Equation 6 can be used to generate random samples of  $\chi_1$  with inverse transform sampling conditioned on either hypothesis  $A$  or hypothesis  $B$ . We denote these samples  $\{\chi_1^j\}_{A, B}$ .

The next step is add values of  $z_1$  to the  $\chi_1$  samples. The marginal prior distribution for  $z_1$  conditioned on  $\chi_1^j$  and hypothesis  $A$  or  $B$  is

$$\begin{aligned} \pi(z_1|\chi_1^j)_{A, B} \\ \propto \frac{1}{n} \sum_k^n \mathcal{I}\left(0 < \frac{\chi_{\text{eff}}^{A, B}(1 + q_{A, B}) - \chi_1^j z_1}{q_{A, B} z_2^k} < 1\right). \end{aligned} \quad (7)$$

This time, the sum over  $k$  is a sum over prior samples for  $z_2$ . We use this distribution to generate random samples  $z_1^j$  given  $\chi_1^j$  (see Fig. 1).<sup>7</sup> Using the same logic, the prior

<sup>6</sup> Probability densities in equations 6, 7, 8 and 10 are normalized manually.

<sup>7</sup> We compute the distribution in Eq. 7 on a two-dimensional grid in  $(z_1, \chi_1)$ . We perform inverse-transform sampling using columns from this grid.

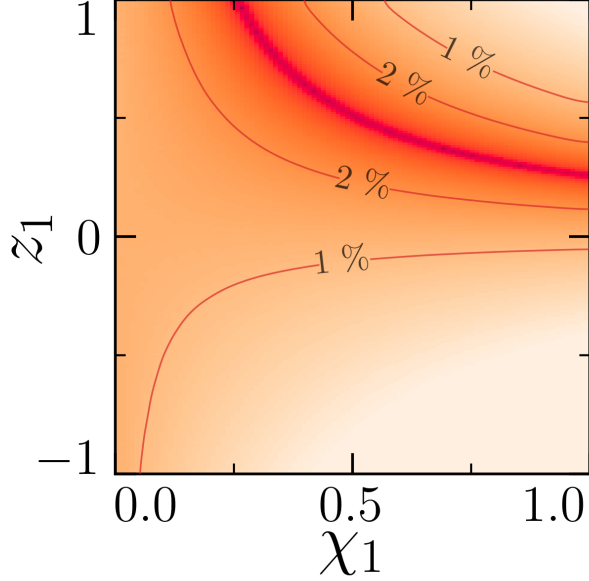


**Figure 1.** Heatmap of  $\pi(z_1, \chi_1 | q, \chi_{\text{eff}})$ . Contours are drawn at the 1% and 2% percentiles. Here,  $(q, \chi_{\text{eff}}) = (0.68, 0.15)$ , corresponding to the high- $q$  point (point A) from Chia et al. 2021, Table I.

distribution for  $z_2$  conditioned on  $\chi_1^j, z_1^j$  and hypothesis  $A$  or  $B$  is

$$\pi(z_2 | \chi_1^j, z_1^j)_{A,B} \propto \mathcal{I} \left( 0 < \frac{\chi_{\text{eff}}^{A,B} (1 + q_{A,B}) - \chi_1^j z_1^j}{q z_2} < 1 \right). \quad (8)$$

This distribution allows us to generate a random sample  $z_2^j$ . For each sample we now have  $\chi_{\text{eff}}, q, \chi_1^j, z_1^j, z_2^j$ , and so the value for  $\chi_2$  is completely determined by Eq. 1.

Using these equations (6-8), we define priors for our stochastic sampler that are conditioned on hypotheses  $A$  and  $B$ .<sup>8</sup> We perform two parameter estimation runs: one for hypothesis  $A$  and one for  $B$ . The evidence from each run yields the marginal likelihood defined in Eq. 3. The ratio of these two evidence values gives us the Bayes factor

$$\text{BF} = \frac{\mathcal{Z}(d|A)}{\mathcal{Z}(d|B)}, \quad (9)$$

which represents the relative probability for hypothesis  $A$  over  $B$  given even prior odds. However, the fiducial LIGO–Virgo prior described above does not assign even prior odds; small values of  $\chi_{\text{eff}}$  are more likely than

larger ones. Thus, to quantify the posterior odds, we now move on to the prior odds:  $\pi_{A,B} = \pi(q_{A,B}, \chi_{\text{eff}}^{A,B})$ .<sup>9</sup>

*The prior odds.* The marginal prior probability density for  $(q, \chi_{\text{eff}})$  can be calculated like so:

$$\pi(q, \chi_{\text{eff}}) \propto \frac{2}{n} \sum_k \left| \frac{1 + q \chi_{\text{eff}}}{\chi_1^k} \right| \left( \frac{\chi_1^k + q \chi_2^k z_2^k}{1 + q} \right). \quad (10)$$

Here, the sum over  $k$  is a sum over fiducial prior samples for  $(\chi_1, \chi_2, z_2)$ . What follows is a derivation of Eq. 10. To begin, we note that

$$\pi(q, \chi_{\text{eff}}) = \pi(\chi_{\text{eff}} | q) \pi(q). \quad (11)$$

We rewrite the first term in terms of marginalisation integrals to obtain

$$\pi(q, \chi_{\text{eff}}) = \int d\chi_1 d\chi_2 dz_2 \pi(\chi_{\text{eff}} | q, \chi_1, \chi_2, z_2) \pi(q, \chi_1, \chi_2, z_2). \quad (12)$$

We have a closed-form expression for the fiducial LIGO–Virgo prior  $\pi(q, \chi_1, \chi_2, z_2)$ . The remaining term in Eq. 12 is related to the fiducial distribution for  $z_1$ . Since  $z_1$  is uniformly distributed,  $\chi_{\text{eff}}$  is uniformly distributed with limits depending on  $(\chi_1, q, \chi_2, z_2)$ :

$$\begin{aligned} \pi(\chi_{\text{eff}} | q, \chi_1, \chi_2, z_2) &= \left| \frac{\partial z_1}{\partial \chi_{\text{eff}}} \right| U \left[ \frac{-\chi_1 + q \chi_2 z_2}{1 + q}, \frac{\chi_1 + q \chi_2 z_2}{1 + q} \right] \\ &= \left| \frac{1 + q \chi_{\text{eff}}}{\chi_1} \right| U \left[ \frac{-\chi_1 + q \chi_2 z_2}{1 + q}, \frac{\chi_1 + q \chi_2 z_2}{1 + q} \right]. \end{aligned} \quad (13)$$

Plugging Eq. 13 into Eq. 12 and replacing the marginalisation integrals with a sum over prior samples, we obtain Eq. 10.

*Sampling.* For hypothesis  $A$  (the high- $q$  peak), we set  $(q, \chi_{\text{eff}}) = (0.68, 0.15)$ . For hypothesis  $B$  (the low- $q$  peak), we set  $(q, \chi_{\text{eff}}) = (0.15, 0.5)$ . These values are chosen to match Table I from Chia et al. (2021) and are plotted in Figure 2. We compute the marginalised likelihood for each hypothesis using `Parallel Bilby` (Ashton et al. 2019; Smith et al. 2020), employing `Dynesty` (Speagle 2020) as our nested sampler (Skilling 2004, 2006). We use 2,000 live points, a data sampling rate of 4096 Hz and the `IMRPhenomXPH` waveform. The complete configuration file for our analyses is located on the github repository for this project (Vajpeyi 2021).

<sup>8</sup> We check the calculations by generating corner plots of our prior samples conditioned on  $A, B$  and comparing them to corner plots created with the fiducial prior, but keeping only samples in the vicinity of  $(q_{A,B}, \chi_{\text{eff}}^{A,B})$ .

<sup>9</sup> For the time being, we duck the question of whether the fiducial LIGO–Virgo prior is a good (astrophysically-motivated) prior. Our short-term goal is simply to compute the posterior odds given that choice of prior.

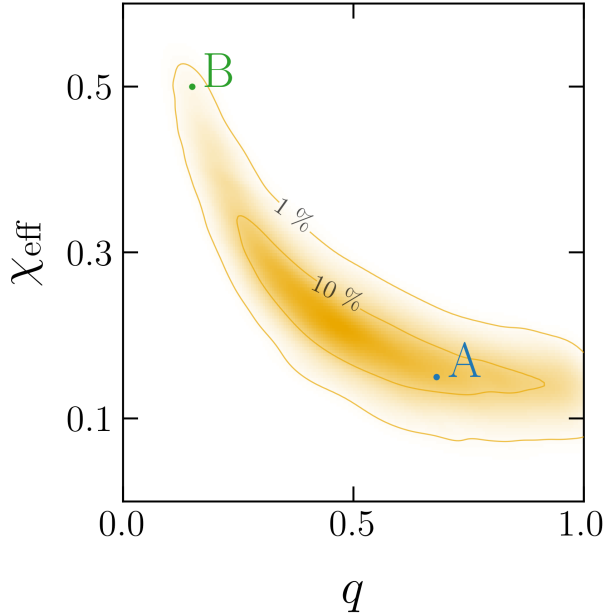


**Figure 2.** Heatmap of the GW151226  $q - \chi_{\text{eff}}$  posterior from Mateu-Lucena et al. (2021)’s analysis. Contours are drawn at the 1% and 10% percentiles. The high- $q$  (blue A) and low- $q$  (green B) points are from Chia et al. 2021, Table I.

### 3. RESULTS

Our findings are summarized in Table 1. We obtain a Bayes factor of 0.3, implying that—if we assign even prior odds to hypotheses  $A$  and  $B$ —the low- $q$  peak is preferred. However, the prior odds are 4.2 in favour of the high- $q$  hypothesis. Thus, we obtain a posterior odds of  $\mathcal{O}_B^A = 1.2$ , implying that the high- $q$  peak is only slightly preferred over the low- $q$  peak. In order to compare this deep follow-up result with the posterior obtained from analyses like those in Abbott et al. (2016), we repeat the analysis from Mateu-Lucena et al. (2021), and apply a kernel density estimate (KDE) of posterior samples in the  $(q, \chi_{\text{eff}})$  plane. The KDE yields a posterior odds of  ${}^K\mathcal{O}_B^A = 7.5$ , suggesting that—for whatever reason—standard LIGO–Virgo analyses significantly underestimate the posterior support for the low- $q$  peak (by a factor of  $\approx 6$ ). At the same time, we find far less support for the low- $q$  peak than (Chia et al. 2021) (by a factor of  $\approx 230$ ).

### 4. DISCUSSION

Increasingly, analyses of gravitational-wave events have contradicting results (e.g. GW151226, GW190425, GW190521 Abbott et al. 2021; Olsen et al. 2022; Nitz et al. 2021), leaving astrophysicists to ponder: which analysis best describes the data? Faulty inferences of events can provide misleading interpretations of the population. In some cases, these analyses differ in software,

**Table 1.** Ratios of marginalised likelihoods, prior odds and posterior odds for the high- $q$  and low- $q$  points.

HIGH-Q vs LOW-Q	
$Z(d A)/Z(d B)$	0.3
$\pi(A)/\pi(B)$	4.2
$\mathcal{O}_B^A$	1.2
${}^K\mathcal{O}_B^A$	7.5

sampler settings, data, waveforms, and noise models, making the determination of the “correct” analysis challenging. The method to compute posterior odds demonstrated in this Letter will help settle debates arising from contradictory results, allowing the community to determine which analysis best represents the posterior distribution.

In this work, we investigate the contradicting interpretations for GW151226. Chia et al. (2021) suggest that the cause for the discrepancy was due to Abbott et al. (2016) not using a sufficiently large number of live points to explore the likelihood surface. However, we hypothesise that the real issue may be the choice of *prior* used for sampling. Past work utilising uniform-in- $\chi_{\text{eff}}$  spin priors have been demonstrated to provide support in regions of parameter space previously unexplored when using the fiducial LIGO–Virgo prior (Olsen et al. 2021; Nitz & Capano 2021). This would not be surprising given that uniform-in-chirp-mass priors are known to provide more efficient sampling than uniform-in-component mass (Romero-Shaw et al. 2020).

In addition to the difference in priors used by Abbott et al. (2016) and Chia et al. (2021), the two analyses differ in the method for estimating noise power spectral density (PSD), the method for estimating the likelihood, the data sampling rates, and the data cleaning methods. Our study’s output can help study the impact of the different techniques on this event. For example, one can study the impact of an alternative PSD by re-weighting the posterior samples for points  $A$  and  $B$  (publicly accessible at Vajpeyi (2021)) with the new PSD.

Our analysis demonstrates that the high- $q$  and low- $q$  likelihood peaks have comparable posterior odds. The high- $q$  mode corresponds to a binary black hole system that is similar to others reported in GWTC-3 (Abbott et al. 2021). However, the low- $q$  mode corresponds to a highly spinning, unequal mass ratio event with non-negligible precession (see Fig. 3). If the binary is indeed described by the low- $q$  mode, this event would be an outlier amongst the other events in the current gravitational wave catalog.



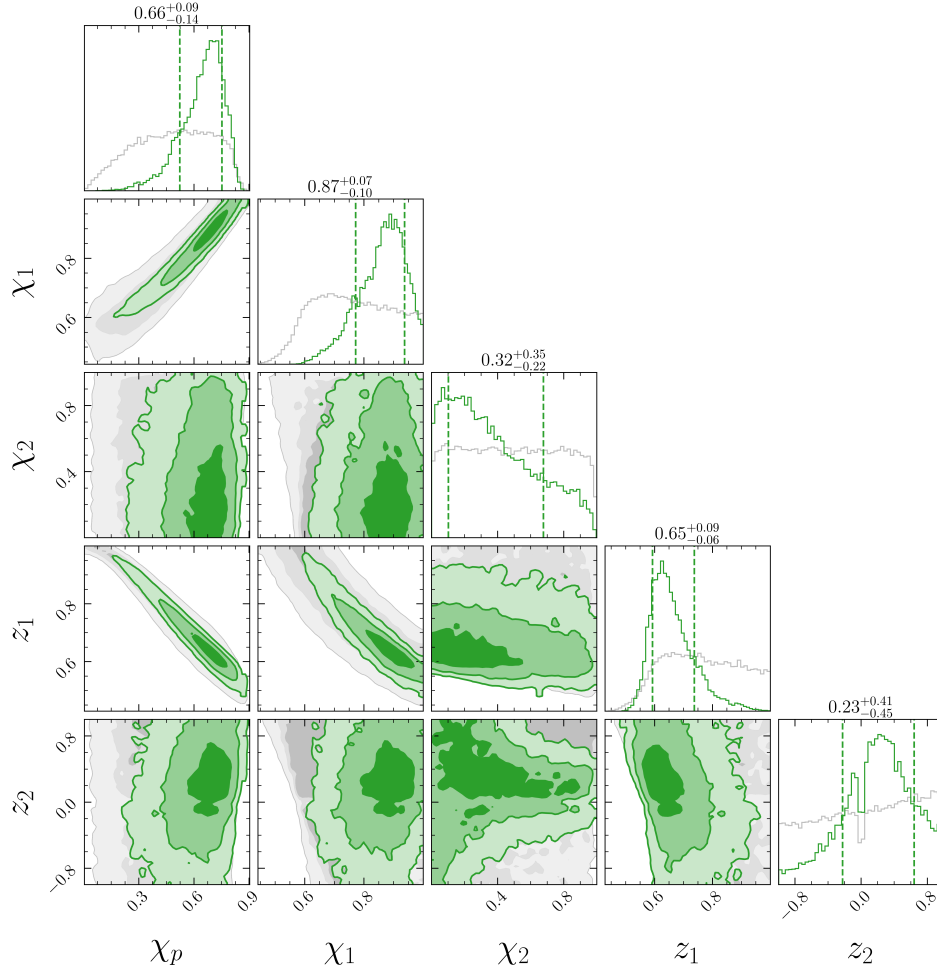


**Figure 3.** Posterior (green) and prior (gray) samples from the low- $q$  (point B) “Deep follow-up” analysis.

It would also be a challenge to explain how this binary formed. The primary black hole from the low- $q$  mode is likely to be highly spinning and misaligned from the orbital plane. This signature is not typical from those expected of the isolated-binary evolution channel; see, e.g., [Qin et al. \(2022\)](#). Dynamical assembly can lead to binaries with large, misaligned primary spin ([Vitale et al. 2017](#); [Rodriguez et al. 2016](#)). However, it may be somewhat challenging to explain the small mass ratio this way since dense stellar environments tend to pair black holes with comparable masses, e.g., ([Dominik et al. 2012](#); [Mapelli et al. 2019](#)). Assembly in active galactic nuclei may account for both the spins and masses of the low- $q$  peak, though, there are significant theoretical uncertainty ([McKernan et al. 2020](#); [Fragione et al. 2019](#)).

Similar to GW151226, there are other events (e.g., GW190425 and GW190521) with alternative interpretations ([Nitz et al. 2020, 2021](#); [Olsen et al. 2021](#)). [Nitz et al.](#)’s analysis of GW190425 resulted in a  $\chi_{\text{eff}}$  slightly

higher than that reported by [Abbott et al. \(2020\)](#). However, this is likely due to the differences in the spin priors used in the analyses—when [Nitz et al.](#) re-weighted their posteriors with a “low-spin” prior, they obtained posteriors comparable with those of [Abbott et al. \(2020\)](#). In the case of GW190521, while [Abbott et al. \(2020b\)](#), [Olsen et al. \(2021\)](#) and [Nitz et al. \(2021\)](#) report the event to have source frame total mass of  $\sim 150 M_{\odot}$ , they also report different values for the event’s mass ratio and spins. [Abbott et al. \(2020b\)](#) report the event to have an almost equal mass ratio  $q \sim 0.79^{+0.19}_{-0.29}$  and negligible spin, while [Nitz et al. \(2021\)](#) and [Olsen et al. \(2021\)](#) report the event to have a bi-modal  $q - \chi_{\text{eff}}$  distribution, with a low- $q$  peak ( $q < 0.3, \chi_{\text{eff}} < 0$ ) and a high- $q$  peak ( $q > 0.3, \chi_{\text{eff}} \sim 0$ ). These bi-modal posteriors may be due to the different mass and spin priors used in the [Abbott et al. \(2020b\)](#) analysis; by using source-frame mass priors and a uniform  $\chi_{\text{eff}}$  prior instead of using detector-frame mass priors and a isotropic spin prior. Determining if there are other events with multi-modal

structures and peaks that have not been accounted is an area worthy of future study.

## 5. ACKNOWLEDGMENTS

The authors gratefully thank Chia *et al.* and Mateu-Lucena *et al.* for sharing their GW151226 posterior samples, and Shanika Galaudage for technical assistance.

We gratefully acknowledge the Swinburne Supercomputing OzSTAR Facility for computational resources. All analyses (inclusive of test and failed analyses) performed for this study used 37.6K core-hours on OzSTAR. This would have amounted to a carbon footprint of  $\sim 2.3\text{t CO}_2$  (Australian Government - Department of the Environment and Energy 2021a,b). However, as OzSTAR is powered by wind energy from Iberdrola Australia; the electricity for computations produce negligible carbon waste.

This material is based upon work supported by NSF’s LIGO Laboratory which is a major facility fully funded by the National Science Foundation. This research has made use of data or software obtained from the Gravitational Wave Open Science Center (gwopenscience.org), a service of LIGO Laboratory, the LIGO Scientific Collaboration, the Virgo Collaboration, and KAGRA. LIGO Laboratory and Advanced LIGO

are funded by the United States National Science Foundation (NSF) as well as the Science and Technology Facilities Council (STFC) of the United Kingdom, the Max-Planck-Society (MPS), and the State of Niedersachsen/Germany for support of the construction of Advanced LIGO and construction and operation of the GEO600 detector. Additional support for Advanced LIGO was provided by the Australian Research Council. Virgo is funded, through the European Gravitational Observatory (EGO), by the French Centre National de Recherche Scientifique (CNRS), the Italian Istituto Nazionale di Fisica Nucleare (INFN) and the Dutch Nikhef, with contributions by institutions from Belgium, Germany, Greece, Hungary, Ireland, Japan, Monaco, Poland, Portugal, Spain. The construction and operation of KAGRA are funded by Ministry of Education, Culture, Sports, Science and Technology (MEXT), and Japan Society for the Promotion of Science (JSPS), National Research Foundation (NRF) and Ministry of Science and ICT (MSIT) in Korea, Academia Sinica (AS) and the Ministry of Science and Technology (MoST) in Taiwan.

This work is supported by the Australian Research Council (ARC) Centre of Excellence CE170100004. AV, RS & ET are supported by the Australian Research Council (ARC) Centre of Excellence CE170100004.

## REFERENCES

- Abbott, B. P., Abbott, R., Abbott, T. D., Abraham, S., & et al. 2020, *ApJ*, 892, L3, doi: [10.3847/2041-8213/ab75f5](https://doi.org/10.3847/2041-8213/ab75f5)
- Abbott, B. P., et al. 2016, *Phys. Rev. Lett.*, 116, 241103
- Abbott, R., Abbott, T. D., Abraham, S., Acernese, F., & et al. 2021, *ApJ*, 913, L7, doi: [10.3847/2041-8213/abe949](https://doi.org/10.3847/2041-8213/abe949)
- Abbott, R., et al. 2020a, *Astrophys. J. Lett.*, 896, L44, doi: [10.3847/2041-8213/ab960f](https://doi.org/10.3847/2041-8213/ab960f)
- . 2020b, *Phys. Rev. Lett.*, 125, 101102, doi: [10.1103/PhysRevLett.125.101102](https://doi.org/10.1103/PhysRevLett.125.101102)
- . 2021
- Acernese, F., et al. 2015, *Classical Quantum Gravity*, 32, 024001, doi: [10.1088/0264-9381/32/2/024001](https://doi.org/10.1088/0264-9381/32/2/024001)
- Ashton, G., Hübner, M., Lasky, P., & Talbot, C. 2019, *Bilby: A User-Friendly Bayesian Inference Library*, 0.4.0, Zenodo, doi: [10.5281/zenodo.2602178](https://doi.org/10.5281/zenodo.2602178)
- Australian Government - Department of the Environment and Energy. 2021a, National Greenhouse Gas Inventory: Quarterly updates, Department of the Environment and Energy. <https://www.industry.gov.au/data-and-publications/national-greenhouse-gas-inventory-quarterly-updates>
- . 2021b, Carbon calculator, Department of the Environment and Energy. <https://www.powershop.com.au/carbon-calculator/>
- Chia, H. S., Olsen, S., Roulet, J., Dai, L., & et al. 2021, arXiv e-prints, arXiv:2105.06486. <https://arxiv.org/abs/2105.06486>
- Dominik, M., Belczynski, K., Fryer, C., Holz, D. E., & et al. 2012, *ApJ*, 759, 52, doi: [10.1088/0004-637X/759/1/52](https://doi.org/10.1088/0004-637X/759/1/52)
- Fragione, G., Grishin, E., Leigh, N. W. C., Perets, H. B., & Perna, R. 2019, *MNRAS*, 488, 47, doi: [10.1093/mnras/stz1651](https://doi.org/10.1093/mnras/stz1651)
- Galaudage, S., Talbot, C., Nagar, T., et al. 2021, *Astrophys. J. Lett.*, 921, L15
- Green, R., Hoy, C., Fairhurst, S., Hannam, M., & et al. 2021, *Phys. Rev. D*, 103, 124023, doi: [10.1103/PhysRevD.103.124023](https://doi.org/10.1103/PhysRevD.103.124023)
- LIGO Scientific Collaboration, Aasi, J., Abbott, B. P., et al. 2015, *Classical and Quantum Gravity*, 32, 074001, doi: [10.1088/0264-9381/32/7/074001](https://doi.org/10.1088/0264-9381/32/7/074001)
- Mandel, I., & Fragos, T. 2020, *ApJ*, 895, L28, doi: [10.3847/2041-8213/ab8e41](https://doi.org/10.3847/2041-8213/ab8e41)

- Mapelli, M., Giacobbo, N., Santoliquido, F., & Artale, M. C. 2019, MNRAS, 487, 2, doi: [10.1093/mnras/stz1150](https://doi.org/10.1093/mnras/stz1150)
- Mateu-Lucena, M., Husa, S., Colleoni, M., Estellés, H., & et al. 2021, arXiv e-prints, arXiv:2105.05960.  
<https://arxiv.org/abs/2105.05960>
- McKernan, B., Ford, K. E. S., & O’Shaughnessy, R. 2020, MNRAS, 498, 4088, doi: [10.1093/mnras/staa2681](https://doi.org/10.1093/mnras/staa2681)
- Nitz, A. H., & Capano, C. D. 2021, ApJ, 907, L9, doi: [10.3847/2041-8213/abccc5](https://doi.org/10.3847/2041-8213/abccc5)
- Nitz, A. H., Capano, C. D., Kumar, S., et al. 2021, arXiv e-prints, arXiv:2105.09151.  
<https://arxiv.org/abs/2105.09151>
- Nitz, A. H., Dent, T., Davies, G. S., et al. 2020, ApJ, 891, 123, doi: [10.3847/1538-4357/ab733f](https://doi.org/10.3847/1538-4357/ab733f)
- Olejak, A., & Belczynski, K. 2021, ApJ, 921, L2, doi: [10.3847/2041-8213/ac2f48](https://doi.org/10.3847/2041-8213/ac2f48)
- Olsen, S., Roulet, J., Chia, H. S., et al. 2021, Physical Review D, 104, doi: [10.1103/physrevd.104.083036](https://doi.org/10.1103/physrevd.104.083036)
- Olsen, S., Venumadhav, T., Mushkin, J., et al. 2022, arXiv e-prints, arXiv:2201.02252.  
<https://arxiv.org/abs/2201.02252>
- Pratten, G., García-Quirós, C., Colleoni, M., et al. 2021, Phys. Rev. D, 103, 104056
- Qin, Y., Wang, Y.-Z., Wu, D.-H., Meynet, G., & et al. 2022, ApJ, 924, 129, doi: [10.3847/1538-4357/ac3982](https://doi.org/10.3847/1538-4357/ac3982)
- Rodriguez, C. L., Zevin, M., Pankow, C., Kalogera, V., & et al. 2016, ApJ, 832, L2, doi: [10.3847/2041-8205/832/1/L2](https://doi.org/10.3847/2041-8205/832/1/L2)
- Romero-Shaw, I. M., Talbot, C., Biscoveanu, S., et al. 2020, MNRAS, 499, 3295, doi: [10.1093/mnras/staa2850](https://doi.org/10.1093/mnras/staa2850)
- Roulet, J., Chia, H.-S., Olsen, S., et al. 2021, Phys. Rev. D, 104, 083010
- Skilling, J. 2004, in American Institute of Physics Conference Series, Vol. 735, Bayesian Inference and Maximum Entropy Methods in Science and Engineering: 24th International Workshop on Bayesian Inference and Maximum Entropy Methods in Science and Engineering, ed. R. Fischer, R. Preuss, & U. V. Toussaint, 395–405, doi: [10.1063/1.1835238](https://doi.org/10.1063/1.1835238)
- Skilling, J. 2006, Bayesian Analysis, 1, 833, doi: [10.1214/06-BA127](https://doi.org/10.1214/06-BA127)
- Smith, R. J. E., Ashton, G., Vajpeyi, A., & Talbot, C. 2020, MNRAS, 498, 4492, doi: [10.1093/mnras/staa2483](https://doi.org/10.1093/mnras/staa2483)
- Speagle, J. S. 2020, MNRAS, 493, 3132, doi: [10.1093/mnras/staa278](https://doi.org/10.1093/mnras/staa278)
- Thrane, E., & Talbot, C. 2019, PASA, 36, e010, doi: [10.1017/pasa.2019.2](https://doi.org/10.1017/pasa.2019.2)
- Vajpeyi, A. 2021, Deep Followup Source Code, <https://github.com/avivajpeyi/deep-gw-pe-followup>, GitHub
- Vitale, S., Gerosa, D., Haster, C.-J., Chatziioannou, K., & et al. 2017, Phys. Rev. Lett., 119, 251103, doi: [10.1103/PhysRevLett.119.251103](https://doi.org/10.1103/PhysRevLett.119.251103)